IEEE Photonics Journal
An IEEE Photonics Society Publication

Open Access

Quantum Receivers for Entanglement Assisted Classical Optical Communications

Volume 13, Number 3, June 2021

Ivan B. Djordjevic, *Fellow, IEEE*

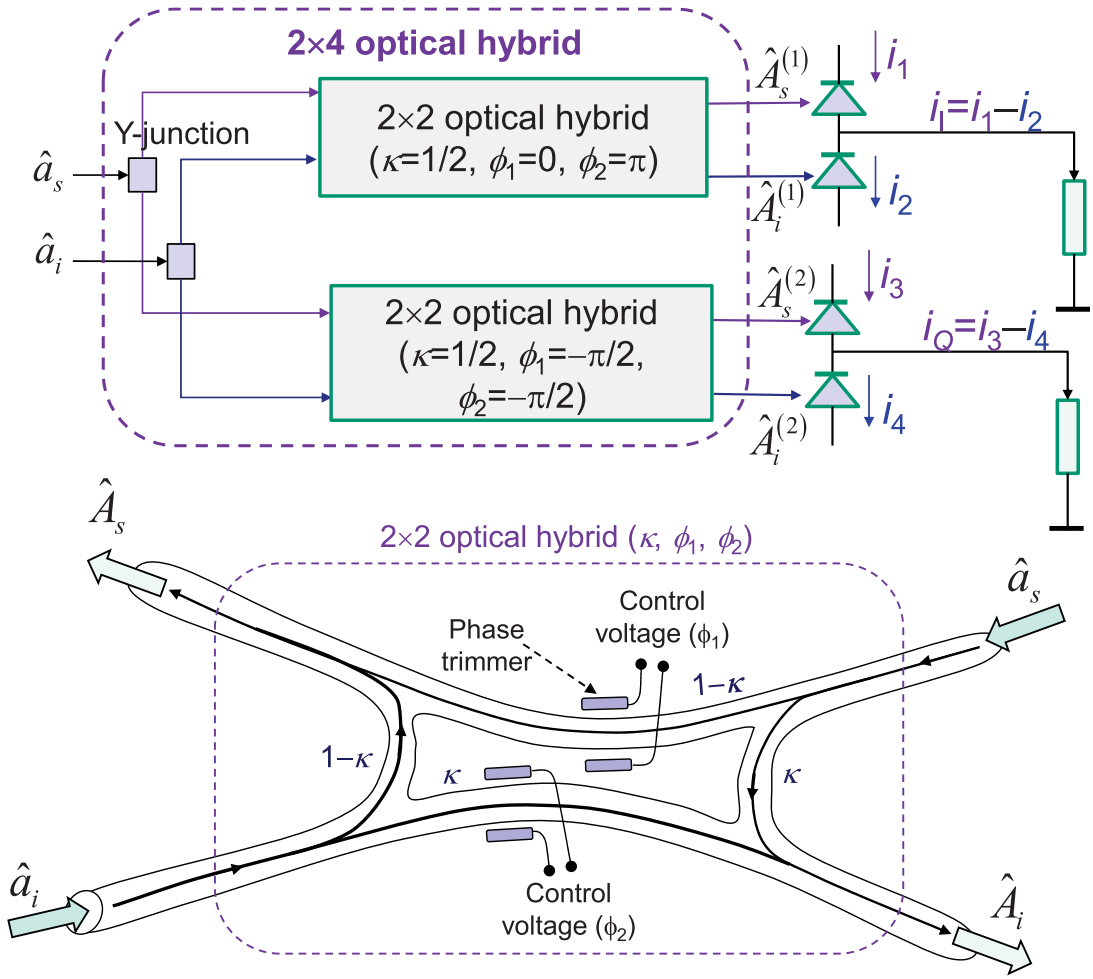

DOI: 10.1109/JPHOT.2021.3075881

Quantum Receivers for Entanglement Assisted Classical Optical Communications

Ivan B. Djordjevic, ***Fellow, IEEE***

University of Arizona, Department of Electrical and Computer Engineering, Tucson, AZ 85721 USA

DOI:10.1109/JPHOT.2021.3075881

Manuscript received April 10, 2021; accepted April 23, 2021. Date of publication April 27, 2021; date of current version May 17, 2021. Corresponding author: Ivan B. Djordjevic (e-mail: ivan@email.arizona.edu).

Abstract: Entanglement assisted (EA) communication represents an interesting alternative to classical communication, in particular in low-brightness and highly noisy regime when it outperforms significantly corresponding classical counterpart in terms of the channel capacity. Even though that the EA capacity is known for decades the optimum quantum receiver has not been determined yet. In this paper, we propose several low-complexity quantum receivers outperforming recently proposed receivers employing the optical parametric amplifier as a basic building block. We demonstrate by simulations that the capacity of the proposed EA schemes, employing Gaussian modulation and the proposed low-complexity joint receivers, can significantly outperform both the Holevo capacity and classical homodyne and heterodyne channel capacities.

Index Terms: Quantum communication, joint quantum receivers, classical communication, entanglement, entanglement assisted capacity, Holevo capacity, Shannon capacity.

1. Introduction

Quantum information processing (QIP) opens new avenues for various applications including high-performance computing, high-precision sensing, and secure communications [1]–[3]. Among various QIP features, the entanglement represents a unique QIP feature: 1) enabling quantum-enhanced sensors with measurement sensitivities exceeding the classical limit, 2) providing certifiable security for data transmissions whose security is guaranteed by the quantum mechanics laws rather than unproven assumptions used in cryptography based on computational security, and 3) enabling quantum computers capable of solving the problems that are numerically intractable for classical computers.

In particular, the pre-shared entanglement can be used to: (i) improve the classical channel capacity [4]–[8], (ii) enable secure communications, (iii) improve sensor sensitivity, (iv) enable distributed quantum computing [9], (v) enable entanglement assisted distributed sensing [10], and (vi) enable provably-secure quantum computer access [11], to mention few. To distribute the entangled signal-idler photon pairs fiber-based quantum network can be used, which is illustrated in Fig. 1.

Even though that the optimum encoding, achieving the entanglement assisted (EA) channel capacity, has been known for decades [4], [5], the design of optimum quantum receiver appears to be still an open problem, although some progress has been made recently [8]. Namely, to achieve

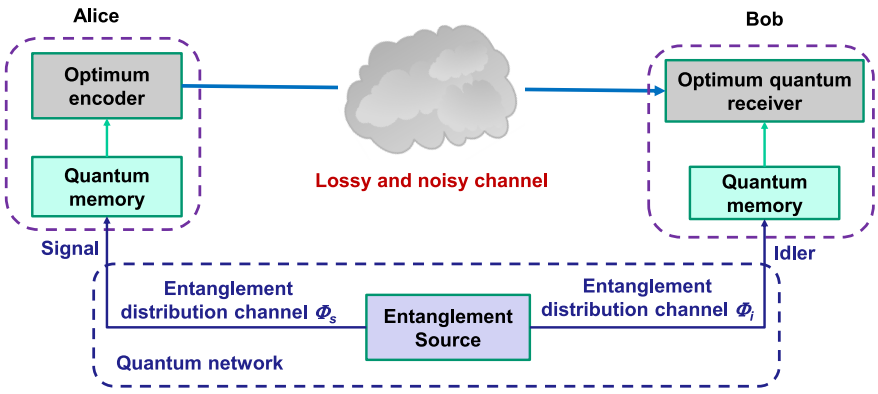

Fig. 1. Illustrating the entanglement assisted classical optical communication concept assuming that entanglement distribution is done through an all-fiber-based quantum network.

the EA capacity it has been shown by Holevo and Werner in [4] that someone needs to use two-mode Gaussian states. From quantum receiver point of view, authors in [8] proposed to use the multiple sections of the feedforward sum-frequency generation (FF-SFG) receiver, initially proposed to detect the target in highly noisy environment [12]. Even though this scheme is suitable for use in quantum binary discrimination problems, it is not an EA channel capacity achieving scheme. Namely, to achieve the EA channel capacity they have transmitted the same binary information over $D = 10^6$ bosonic modes thus occupying the whole C and L bands as well as the portion of S band.

In this paper, we first describe the optimum encoding based on Gaussian modulation (GM) of the signal photon in two-mode-squeezed-vacuum (TMSV) state as well as a generic EA communication system of interest. We then review recent quantum detector proposals employing the optical parametric amplifier (OPA) as the basic building block in corresponding joint receivers. We then describe proposed joint receiver schemes that can achieve comparable or better performance, while being of lower complexity and not requiring the OPA as the building block. We then evaluate by simulations the performance of the proposed EA scheme, employing the Gaussian modulation of signal mode and the proposed joint receiver, and demonstrate significant channel capacity improvements over corresponding Holevo, homodyne, and heterodyne channel capacities.

The paper is organized as follows. The realistic entanglement assisted optical communication systems of interests are described in Section 2. In Section 3, we describe two recently proposed [8] nonlinear receivers suitable for EA communication. The proposed joint receivers of low complexity are described in Section 4. In Section 5 we demonstrate that the capacity of the EA scheme with GM and the proposed joint receiver significantly outperforms the Holevo capacity and classical homodyne and heterodyne capacities. Some relevant concluding remarks are given in Section 6.

2. Entanglement Assisted Classical Optical Communication Systems

As illustrated in Fig. 1, all-fiber based quantum network is used to distribute the entangled states, which are stored in quantum memories and used when needed. Alice employs her signal photon of entangled pair and transmits the classical data, imposed on the signal photon over lossy and noisy quantum channel. On receiver side, Bob employs the entangled idler photon to decide on what was transmitted on signal photon in an optimum quantum receiver.

The corresponding model for EA classical communication is provided in Fig. 2, where the pre-shared entanglement is distributed with the help of two channels: signal channel, denoted by Φ_s, and the idler channel, denoted by Φ_i. We assume that quantum error correction is applied to protect the quantum states stored in quantum memories against decoherence effects. The Alice-to-Bob

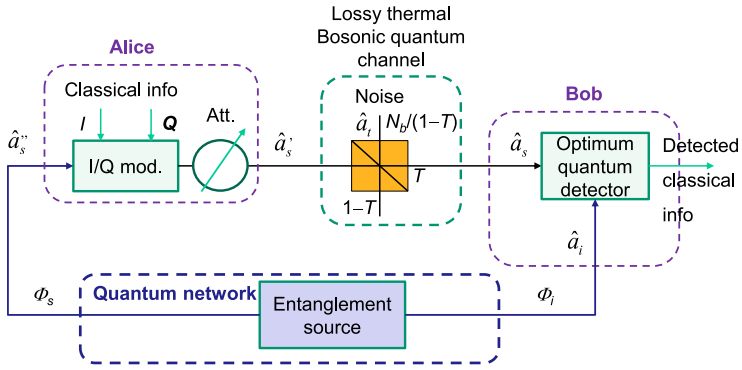

Fig. 2. Illustrating the entanglement assisted classical communication system model. I/Q mod: I/Q modulator, Att.: attenuator (it is optional).

(main) channel is modelled by the single-mode thermal lossy Bosonic channel model

$$\hat{a}_s = \sqrt{T}\hat{a}_s + \sqrt{1-T}\hat{a}_b, \tag{1}$$

where T is the transmissivity of the main channel, while $\hat{a}_b$ is a thermal (background) mode with the mean photon number being $N_b/(1-T)$. Evidently this channel can also be interpreted as a zero-mean additive white Gaussian noise (AWGN) channel with power-spectral density of N_b and attenuation coefficient being T. Alice modulates the signal mode $\hat{a}_s$ with the help of an I/Q modulator, as shown in Fig. 2, by performing the Gaussian modulation (GM).

We further assume that two-mode Gaussian states, to be used in EA communication, are generated by the continuous-wave spontaneous parametric down-converter (SPDC) entangled-photon source. The SPDC-based entangled source is a broadband source with $D = T_m W$ i.i.d. signal-idler mode pairs, with W being the phase-matching bandwidth and T_m is the measurement interval. Each signal-idler mode pair, with corresponding signal and idler annihilation operators being $\hat{a}_s$ and $\hat{a}_i$, is in fact a two-mode squeezed vacuum (TMSV) state whose representation in Fock basis is given by

$$|\psi\rangle_{s,i} = \frac{1}{\sqrt{N_s+1}} \sum_{n=0}^{\infty} \left(\frac{N_s}{N_s+1}\right)^{n/2} |n\rangle_s |n\rangle_i, \tag{2}$$

where $N_s = \langle \hat{a}_s^\dagger \hat{a}_s \rangle = \langle \hat{a}_i^\dagger \hat{a}_i \rangle$ denotes the mean photon number per mode. The signal-idler entanglement is specified by the phase-sensitive cross-correlation (PSCC) $C_{si} = \langle \hat{a}_s^\dagger \hat{a}_i \rangle = \sqrt{N_s(N_s+1)}$, between signal and idler, which represents the quantum limit. The TMSV is a pure maximally entangled zero-mean Gaussian state with Wigner covariance matrix being:

$$\mathbf{\Sigma}_{TMSV} = \begin{bmatrix} (2N_s+1)\,\mathbf{1} & 2\sqrt{N_s(N_s+1)}\mathbf{Z} \\ 2\sqrt{N_s(N_s+1)}\mathbf{Z} & (2N_s+1)\,\mathbf{1} \end{bmatrix}, \tag{3}$$

where $\mathbf{1}$ is the identity matrix and $\mathbf{Z} = \mathrm{diag}(1, -1)$ is the Pauli Z-matrix. Clearly, in low-brightness regime $N_s << 1$, the PSCC is $C_{si} \approx \sqrt{N_s}$ that is much larger than the classical limit N_s. The coordinates for the GM are generated from a zero-mean 2-D Gaussian distribution in the digital domain, a digital-to- analog converter (DAC) is used to represent the samples, which are further used as RF inputs of the I/Q modulator. The Gaussian samples are properly scaled to account for the I/Q modulator insertion loss such that average number of transmitted signal photons per mode is equal to $N_s = \langle (\hat{a}_s)^\dagger \hat{a}_s \rangle$.

Given that the action of the beam splitter (BS), describing the quantum channel, can be represented by the following matrix representation $BS(\tau) = \begin{bmatrix} \sqrt{\tau}\mathbf{1} & \sqrt{1-\tau}\mathbf{1} \\ -\sqrt{1-\tau}\mathbf{1} & \sqrt{\tau}\mathbf{1} \end{bmatrix}$, in order to determine

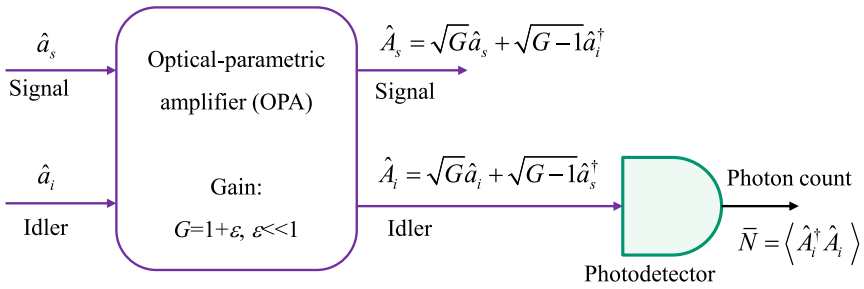

Fig. 3. The operation principle of OPA based receiver. The photons are detected at the port where idler is amplified.

the covariance matrix after the beam splitter in entanglement distribution channel (see Fig. 2) we need to apply the following sympletic operation [1]–[3] by

$$BS_c(T) = \mathbf{1} \oplus BS(T) = \begin{bmatrix} \mathbf{1} & \mathbf{0} & \mathbf{0} \\ \mathbf{0} & \sqrt{T}\mathbf{1} & \sqrt{1-T}\mathbf{1} \\ \mathbf{0} & -\sqrt{1-T}\mathbf{1} & \sqrt{T}\mathbf{1} \end{bmatrix} \tag{4}$$

on the input covariance matrix $\mathbf{\Sigma}_{TMSV}$ to obtain:

$$\mathbf{\Sigma}' = BS_c(T) \begin{bmatrix} \mathbf{\Sigma}_{TMSV} & \mathbf{0} \\ \mathbf{0} & \sigma'^2\mathbf{1} \end{bmatrix} [BS_c(T)]^T, \tag{5}$$

where the variance of thermal state is $N_b/(1-T)$ thermal photons. By keeping Alice and Bob submatrices, and ignoring the rest, we obtain the following covariance matrix:

$$\mathbf{\Sigma}_{AB} = \begin{bmatrix} (2N_s+1)\mathbf{1} & 2\sqrt{TN_s(N_s+1)}\mathbf{Z} \\ 2\sqrt{TN_s(N_s+1)}\mathbf{Z} & (2N_s'+1)\mathbf{1} \end{bmatrix}, \tag{6}$$

where $N_s' = N_sT + N_b$.

3. Nonlinear Receivers Based Entanglement Assisted Communication

The joint measurement receiver may use the optical parametric optical amplifier (OPA), shown in Fig. 3, wherein the gain is selected as $G = 1+\varepsilon$, $\varepsilon << 1$. The idler output of the OPA is given by [13]

$$\hat{A}_i = \sqrt{G}\,\hat{a}_i + \sqrt{G-1}\,\hat{a}_s^\dagger. \tag{7}$$

Assuming that M-ary PSK is imposed by the I/Q modulator, the signal mode at the output modulator $\hat{a}_s$ is related to the input mode of modulator $\hat{a}_s'$ by $\hat{a}_s = e^{j\varphi}\hat{a}_s'$ where φ is the phase shift introduced by the modulator. The photodetector output operator is given by:

$$\hat{I} = RA_i^\dagger \hat{A}_i = R\left(\sqrt{G}\,\hat{a}_i^\dagger + \sqrt{G-1}\,\hat{a}_s\right)\left(\sqrt{G}\,\hat{a}_i + \sqrt{G-1}\,\hat{a}_s^\dagger\right)$$

$$= R\left[G\hat{a}_i^\dagger\hat{a}_i + \sqrt{G(G-1)}\hat{a}_i^\dagger e^{-j\varphi}(\hat{a}_s')^\dagger + \sqrt{G(G-1)}e^{j\varphi}\hat{a}_s'\hat{a}_i' + (G-1)\underbrace{\hat{a}_s''(\hat{a}_s')^\dagger}_{(\hat{a}_s')^\dagger\hat{a}_s''+\mathbf{1}}\right], \tag{8}$$

where R is the photodiode responsivity. Without loss of generality and given that we are concerned with fundamental limits, in the rest of this paper we will assume that $R = 1$ A/W. The expected value

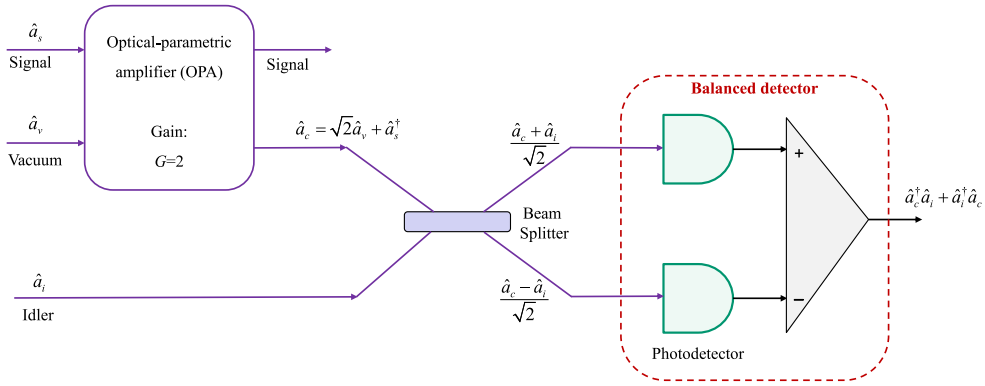

Fig. 4. The operation principle of the OPC receiver.

of the photocurrent operator is related to the photon count average by:

$$\left\langle \hat{i} \right\rangle = \left\langle A_i^\dagger \hat{A}_i \right\rangle = GN_i + e^{-j\varphi}\sqrt{G(G-1)}C_{si} + e^{j\varphi}\sqrt{G(G-1)}C_{si} + (G-1)\left(N_s'' + 1\right)$$
$$= GN_s + 2\sqrt{G(G-1)}C_{si}\cos\varphi + (G-1)\left(N_s'' + 1\right), \tag{9}$$

where we used that $N_i = N_s$ for TMSV state. The second line of this expression matches the Eq. (17) provided in ref. [8]. Clearly, the photocurrent average is proportional to cosφ and we can detect the transmitted phase, but they are also two shot noise terms. Similarly to previous EA communication papers [4]–[8], and since we are concerned with ultimate channel capacity limits, we ignore the OPA imperfections.

Given that OPA receiver is not suitable for balanced detection, we can use instead the *optical phase-conjugate* (OPC) receiver shown in Fig. 4. Here we use the OPA to nonlinearly interreact the signal mode $\hat{a}_s$with the vacuum mode $\hat{a}_v$ to get the following output at the idler port $\hat{a}_c = \sqrt{G}\,\hat{a}_v + \sqrt{G-1}\,\hat{a}_s^\dagger$, which for gain $G = 2$ is simply $\hat{a}_c = \sqrt{2}\,\hat{a}_v + \hat{a}_s^\dagger$. Now by performing the mixing of the a_c-mode with the idler mode on a balanced beam splitter (BBS) followed by the balanced detection (BD), we obtain the following BD photocurrent operator:

$$\begin{aligned}\hat{i}_{BD} &= \tfrac{1}{2}\left(\hat{a}_c^\dagger + \hat{a}_i^\dagger\right)\left(\hat{a}_c + \hat{a}_i\right) - \tfrac{1}{2}\left(\hat{a}_c^\dagger - \hat{a}_i^\dagger\right)\left(\hat{a}_c - \hat{a}_i\right) \\ &= \hat{a}_c^\dagger\hat{a}_i + \hat{a}_i^\dagger\hat{a}_c,\end{aligned} \tag{10}$$

and after substituting the expression for a_c-mode we obtain:

$$\hat{i}_{BD} = \sqrt{2}\hat{a}_v^\dagger\hat{a}_i + \hat{a}_s\hat{a}_i + \sqrt{2}\hat{a}_i^\dagger\hat{a}_v + \hat{a}_i^\dagger\hat{a}_s^\dagger. \tag{11}$$

For M-ary PSK we have that $\hat{a}_s = e^{j\varphi}\hat{a}_s'$, and given that the vacuum mode and the idler mode are uncorrelated we obtain the following expression for the expectation of the BD photocurrent operator:

$$\left\langle \hat{i}_{BD} \right\rangle = e^{j\phi}\underbrace{\left\langle \hat{a}_s'\hat{a}_i \right\rangle}_{C_{si}} + e^{-j\phi}\underbrace{\left\langle \hat{a}_i^\dagger\hat{a}_s^\dagger \right\rangle}_{C_{si}} = 2C_{si}\cos\varphi, \tag{12}$$

thus canceling the noise terms in single-detector case [see Eq. (9)]. The variance of the BD photocurrent operator will be:

$$\begin{aligned}Var\left(\hat{i}_{BD}\right) &= \left\langle \hat{i}_{BD}^2 \right\rangle - \left\langle \hat{i}_{BD} \right\rangle^2 \\ &= N_iN_s' + (N_i+1)\left(N_s'+1\right) + 2C_{si}^2\cos(2\varphi) - 4C_{si}^2\cos^2\varphi.\end{aligned} \tag{13}$$

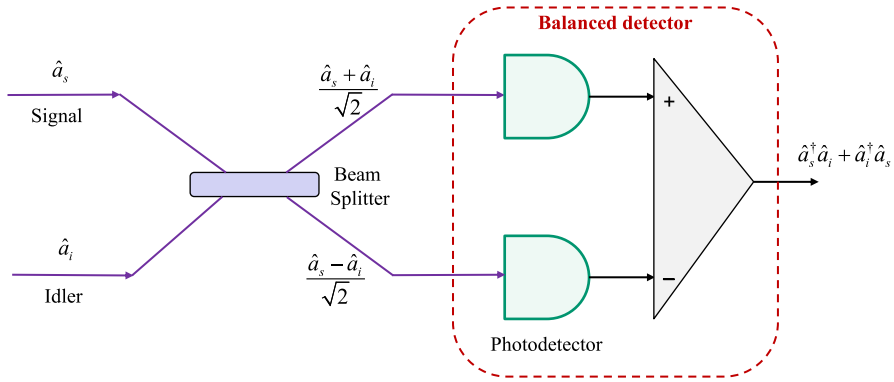

Fig. 5. The BBS based joint balanced detection receiver.

For binary PSK (BPSK) the expression for variance simplifies to:

$$Var^{(\mathrm{BPSK})}\left(\hat{i}_{BD}\right) = N_i N_s' + \left(N_i+1\right)\left(N_s'+1\right) - 2C_{si}^2. \tag{14}$$

Further, in low-brightness and highly noisy regime where $N_s<<1$ and $N_b>>1$, we obtain the following expression for variance:

$$Var^{(\mathrm{BPSK})}\left(\hat{i}_{BD}\right) \approx \left(2N_s+1\right)N_b. \tag{15}$$

The corresponding expression for bit error probability will be:

$$P_b^{(\mathrm{BPSK})} = \frac{1}{2}erfc\left(\sqrt{\frac{4TN_s\left(N_s+1\right)}{\left(2N_s+1\right)N_b}}\right), \tag{16}$$

where we used erfc(·) to denote the complementary error function, defined by $erfc(u) = (2/\sqrt{\pi})\int_u^\infty \exp(-x^2)dx$. For $N_s<<1$ and $N_b>>1$ this expression agrees with the Eqs. (C1), (C2) of ref. [8].

Given that the SPDC-based entangled source is broadband source, by employing D modes all modulated with the same BPSK signal, the bit error probability can be reduced:

$$P_b^{(\mathrm{BPSK})}(D) = \frac{1}{2}erfc\left(\sqrt{\frac{4DTN_s\left(N_s+1\right)}{\left(2N_s+1\right)N_b}}\right). \tag{17}$$

The corresponding binary symmetric channel capacity per mode will be:

$$C_{OPC}^{(\mathrm{BPSK})} = \frac{1}{D}\left[1-h\left(P_b^{(\mathrm{BPSK})}(D)\right)\right], \tag{18}$$

where $h(x)$ is the binary entropy function, defined by $h(x) = -x\log_2 x - (1-x)\log_2(1-x)$.

4. Proposed Joint Receivers for Entanglement Assisted Communication

By close inspection of Eqs. (10) and (11) for the OPC receiver, we conclude that we exploited the fact that there is no correlation between the signal and vacuum modes and what really matters is the mixing of the signal and idler modes on the BBS. This indicates that the OPA is not really needed, we can mix the signal and idler modes directly on BBS as shown in Fig. 5. The BD photocurrent operator is now simply:

$$\hat{i}_{BD} = \hat{a}_s^\dagger\hat{a}_i + \hat{a}_i^\dagger\hat{a}_s, \tag{19}$$

and for M-ary PSK the expressions (12)–(18) for OPC receiver, proposed in [8], are directly applicable here. This receiver is identical to the coherent detection receiver, wherein instead of the local oscillator (LO) laser signal, the idler mode is used. Therefore, different coherent detection receivers described in [14] (see Section 6.8.1) are directly applicable. Now we describe an optical hybrid (OH) based joint balanced detection scheme, shown in Fig. 6, because it is suitable for implementation in integrated optics and as such is compatible with the quantum nanophotonics. In Fig. 6(a), we provide the configuration of 2 × 2 optical hybrid-based BD, while in Fig. 6(b) we provide the corresponding integrated optics implementation of 2 × 2 OH. The OH has two phase trimmers to introduce the phase shifts ϕ_1 and ϕ_2, respectively.

The optical hybrid is composed of two input and two output Y-junctions, and the scattering matrix can be described by:

$$\boldsymbol{S} = \begin{bmatrix} e^{j\phi_1}\sqrt{1-\kappa} & \sqrt{1-\kappa} \\ \sqrt{\kappa} & e^{j\phi_2}\sqrt{\kappa} \end{bmatrix} \tag{20}$$

where κ is the power splitting ratio of Y-junctions, and this matrix transforms input signal and idler modes to:

$$\begin{bmatrix} \hat{A}_s \\ \hat{A}_i \end{bmatrix} = \boldsymbol{S}\begin{bmatrix} \hat{a}_s \\ \hat{a}_i \end{bmatrix}. \tag{21}$$

In particular, for the power splitting ratio $\kappa = 1/2$ this transformation is simply:

$$\begin{bmatrix} \hat{A}_s \\ \hat{A}_i \end{bmatrix} = \frac{1}{\sqrt{2}}\begin{bmatrix} e^{j\phi_1} & 1 \\ 1 & e^{j\phi_2} \end{bmatrix}\begin{bmatrix} \hat{a}_s \\ \hat{a}_i \end{bmatrix}. \tag{22}$$

Assuming that arbitrary 2-D constellation is used, the signal mode at the output of I/Q modulator $\hat{a}_s$ is related to the input mode of modulator $\hat{a}_s'$ by $\hat{a}_s = s\hat{a}_s'$,where $s = s_\mathrm{I} + \mathrm{j}s_\mathrm{Q}$ is the 2-D signal constellation point. For instance for M-ary PSK, we have that $s = \exp(\mathrm{j}\varphi)$. Based on Fig. 6(a), we obtain the following balanced detector photocurrent operator:

$$\hat{i}_{BD} = \frac{1}{2}s^\dagger\left(e^{-j\phi_1} - e^{j\phi_2}\right)(a_s')^\dagger a_i + \frac{1}{2}s\left(e^{j\phi_1} - e^{-j\phi_2}\right)a_i^\dagger a_s'. \tag{23}$$

The expectation of photocurrent operator is given by:

$$\left\langle \hat{i}_{BD} \right\rangle = \frac{1}{2}s^\dagger C_{si}\left(e^{-j\phi_1} - e^{j\phi_2}\right) + \frac{1}{2}s\left(e^{j\phi_1} - e^{-j\phi_2}\right)C_{si}. \tag{24}$$

In special case, by setting $\phi_1 = 0$ rad and $\phi_2 = \pi$, we obtain the following mean of BD photocurrent operator:

$$\left\langle \hat{i}_{BD}^{(I)} \right\rangle = 2C_{si}\underbrace{\mathrm{Re}\{s\}}_{s_I} = 2C_{si}s_I, \tag{25}$$

thus detecting the in-phase component s_I of transmitted signal constellation point. Clearly, for M-ary PSK Re{s} = cosφ thus obtaining the Eq. (12). On the other hand, by setting $\phi_1 = -\pi/2$ and $\phi_2 = -\pi/2$, we obtain the following mean of BD photocurrent operator:

$$\left\langle \hat{i}_{BD}^{(Q)} \right\rangle = 2C_{si}\underbrace{\mathrm{Im}\{s\}}_{s_Q} = 2C_{si}s_Q, \tag{26}$$

thus detecting the quadrature component s_Q of transmitted signal constellation point. Therefore, the joint receiver shown in Fig. 6(a) can be used to determine in-phase and quadrature components by properly setting the control voltages on phase trimmers. The variance of BD photocurrent operator is given by:

$$Var\left(\hat{i}_{BD}\right) = \left\langle \hat{i}_{BD}^2 \right\rangle - \left\langle \hat{i}_{BD} \right\rangle^2 = \frac{1}{4}\left|e^{j\phi_1} - e^{-j\phi_2}\right|^2\left(2N_s'N_i + N_s' + N_i\right)$$

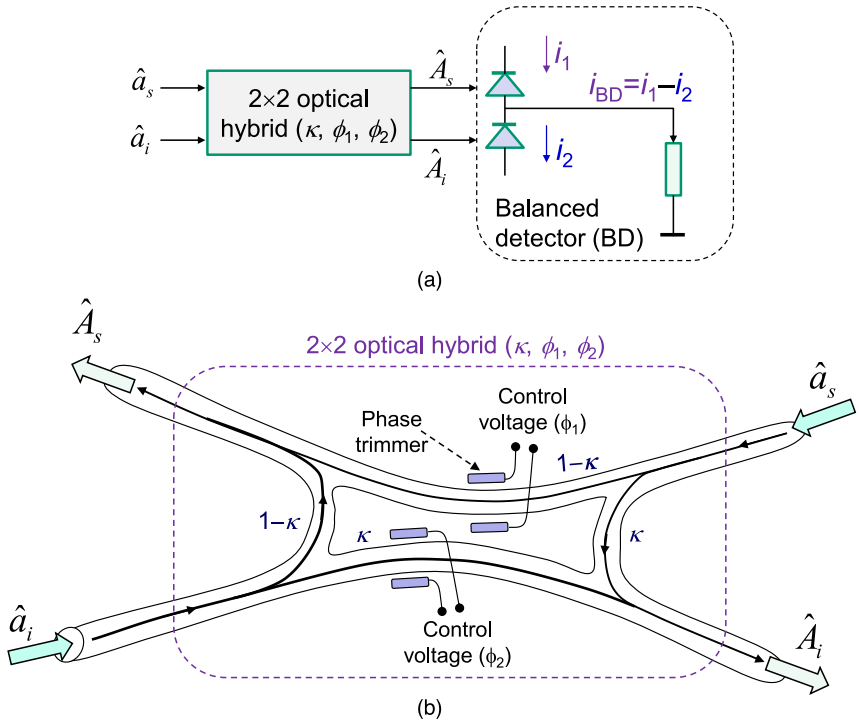

Fig. 6. The 2 × 2 optical hybrid based joint balanced detection receiver: (a) receiver configuration and (b) 2 × 2 optical hybrid implementation in integrated optics.

$$+\frac{C_{si}^2}{4}\left[\left(\left\langle s^{\dagger 2}\right\rangle - s^{\dagger 2}\right)\left(e^{-j\phi_1}-e^{j\phi_2}\right)^2\right]+\frac{C_{si}^2}{4}\left[\left(\left\langle s^2\right\rangle - s^2\right)\left(e^{j\phi_1}-e^{-j\phi_2}\right)^2\right]$$
$$-\frac{C_{si}^2}{2}s^{\dagger}s\left|e^{j\phi_1}-e^{-j\phi_2}\right|^2, \tag{27}$$

which is clearly dependent on signal constellation-point. In special case, by setting $\phi_1 = 0$ rad and $\phi_2 = \pi$, we obtain the following variance of BD photocurrent operator:

$$Var\left(\hat{i}_{BD}^{(I)}\right) = 2N_s N_i + N_s + N_i + C_{si}^2\left(\left\langle s^{\dagger 2}\right\rangle - s^{\dagger 2}\right) + C_{si}^2\left(\left\langle s^2\right\rangle - s^2\right) - 2C_{si}^2 s^{\dagger}s. \tag{28}$$

On the other hand, by setting $\phi_1 = -\pi/2$ and $\phi_2 = -\pi/2$, we obtain the following variance of BD photocurrent operator:

$$Var\left(\hat{i}_{BD}^{(Q)}\right) = 2N_s N_i + N_s + N_i - C_{si}^2\left(\left\langle s^{\dagger 2}\right\rangle - s^{\dagger 2}\right) - C_{si}^2\left(\left\langle s^2\right\rangle - s^2\right) - 2C_{si}^2 s^{\dagger}s. \tag{29}$$

To simultaneously detect the in-phase and quadrature components, we need to use the 2 × 4 optical hybrid-based joint receiver shown in Fig. 7. The upper branch and BD are used to detect the in-phase component, while the lower branch and BD are used to detect the quadrature component. Given that two additional Y-junctions are needed, one for signal mode and the second for idler mode, we need to adjust the transmit TMSV state so that the Eqs. (25) and (26) can be used to describe mean photocurrents corresponding to in-phase and quadrature components, while Eqs. (28) and (29) to describe the corresponding variances.

The corresponding 3 dB directional couplers-based implementation of the joint receiver is provided in Fig. 8.

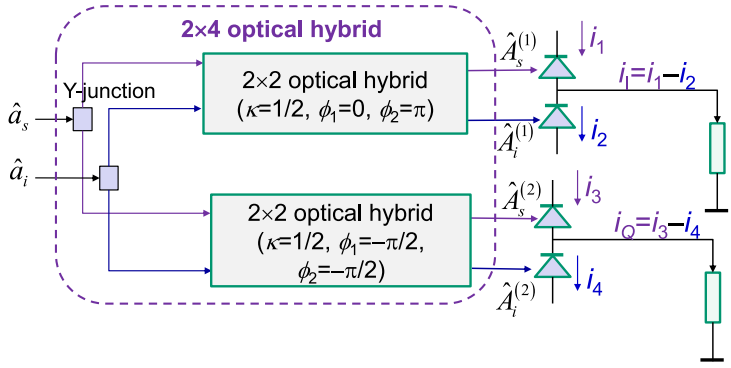

Fig. 7. The 2 × 4 optical hybrid based joint receiver suitable for demodulation of arbitrary 2-D constellation.

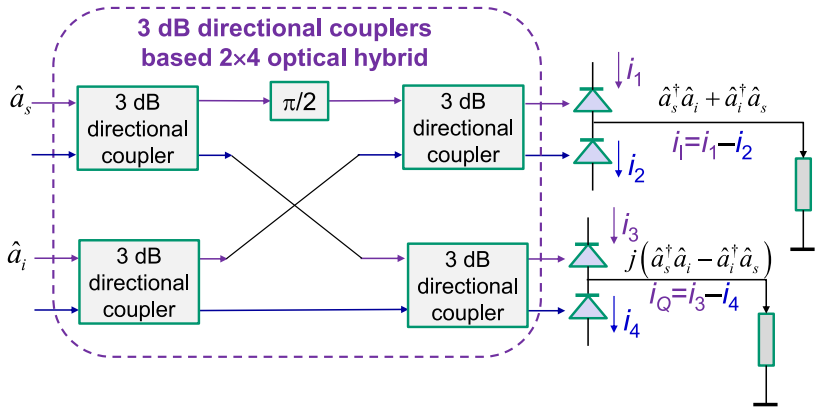

Fig. 8. The joint receiver suitable for demodulation of arbitrary 2-D constellation implemented using 3 dB directional couplers-based 2 × 4 optical hybrid.

The scattering matrix of 3 dB directional coupler is given by [14] $\boldsymbol{S} = 2^{-1/2}\begin{bmatrix} 1 & j \\ j & 1 \end{bmatrix}$. Given that vacuum states at unused input ports of 3 dB directional couplers are not correlated to the signal and idler modes, corresponding correlations at balanced detector outputs will be zeros, and to simplify derivation we can ignore the vacuum states. Following similar procedure as in text related to the Fig. 6, we obtain the following balanced photocurrent operators for in-phase and quadrature components:

$$\hat{i}_{BD}^{(I)} = \hat{a}_s^\dagger \hat{a}_i + \hat{a}_i^\dagger \hat{a}_s, \tag{30a}$$

$$\hat{i}_{BD}^{(Q)} = j\left(\hat{a}_s^\dagger \hat{a}_i - \hat{a}_i^\dagger \hat{a}_s\right). \tag{30b}$$

Again, assuming that arbitrary 2-D constellation is used, the signal mode at the output of I/Q modulator $\hat{a}_s$ is related to the input mode of modulator $\hat{a}_s'$ by $\hat{a}_s = s\hat{a}_s'$, so that the corresponding expectations become:

$$\begin{aligned} \left\langle \hat{i}_{BD}^{(I)} \right\rangle &= \left\langle s^\dagger (\hat{a}_s')^\dagger \hat{a}_i + s\hat{a}_i^\dagger \hat{a}_s' \right\rangle = \left(s^\dagger + s\right) C_{si} \\ &= 2\mathrm{Re}\{s\} C_{si} = 2 s_I C_{si}, \end{aligned} \tag{31a}$$

$$\left\langle \hat{i}_{BD}^{(Q)} \right\rangle = \left\langle j\left(s^{\dagger}(\hat{a}_s^{\cdot})^{\dagger}\hat{a}_i - s\hat{a}_i^{\dagger}\hat{a}_s^{\cdot}\right)\right\rangle = j\left(s^{\dagger} - s\right)C_{si}$$
$$= 2\mathrm{Im}\{s\}C_{si} = 2s_Q C_{si}, \tag{31b}$$

which are proportional to the in-phase s_I and quadrature s_Q components of transmitted signal constellation points. Given that equations in (31) are identical to Eqs. (25) and (26) the variances will be the same as well, and the performance of scheme shown in Fig. 8 will be the identical to that shown in Fig. 7.

5. Performance of Proposed Entanglement Assisted Communication Schemes

For Gaussian modulation we described in Section 2 and 2 × 4 optical hybrid based joint receiver shown in Fig. 7, the corresponding channel capacity will be:

$$C = \log_2\left(1 + \frac{4TN_s(N_s+1)\left(s_I^2+s_Q^2\right)}{2\left(2N_s^{\cdot}N_i + N_s^{\cdot} + N_i\right) - 4C_{si}^2 s^{\dagger}s}\right) = \log_2\left(1 + \frac{2TN_s(N_s+1)\left(s_I^2+s_Q^2\right)}{2N_s^{\cdot}N_s + N_s^{\cdot} + N_s - 2C_{si}^2 s^{\dagger}s}\right). \tag{32}$$

From Holevo's papers [4], [5] we know that the quantum limit of classical capacity is given by:

$$C_{\text{Holevo}} = g(TN_s + N_b) - g(N_b), \tag{33}$$

which is also known as the *Holevo capacity*, wherein $g(x) = (x+1)\log_2(x+1) - x\log_2 x$.

Given that according to the uncertainty principle both in-phase and quadrature components of a Gaussian state cannot be simultaneously measured with the complete precision, for homodyne detection the information is encoded on a single quadrature so that the average number of received photon is $4TN_s$, while the average number of noise photons is $2N_b+1$, and the corresponding classical capacity for homodyne detection is $C_{\text{hom}} = 0.5\log_2[1 + 4TN_s/(2N_b+1)]$. On the other hand, in heterodyne detection both quadratures are used so that the average number of received signal photons will be $0.5*0.5*4TN_s = TN_s$ (one-half comes from splitting to two quadratures and second half from heterodyne splitting), while the average number of noise photons per quadrature is $(2N_b+1)/2+1/2 = N_b+1$. The corresponding heterodyne channel capacity will be $C_{het} = \log_2[1 + TN_s/(N_b+1)]$. To achieve the channel capacity in classical case we need to use the GM by generating samples from two uncorrelated zero-mean Gaussian sources and with the help of an arbitrary waveform generator (AWG) impose them on the optical carrier by using an I/Q modulator. To achieve the Holevo capacity we need to use the Gaussian state. For instance, the coherent state with GM can achieve the Holevo capacity.

Regarding the EA capacity, by close inspection of Eq. (6) we conclude that this covariance matrix has the standard form [15]–[19] $\boldsymbol{\Sigma} = \begin{bmatrix} a\mathbf{1} & \boldsymbol{C} \\ \boldsymbol{C} & b\mathbf{1} \end{bmatrix}$ with $a = 2N_s + 1$, $b = 2N_s^{\cdot} + 1$, $\boldsymbol{C} = c\boldsymbol{Z}$, $c = 2\sqrt{TN_s(N_s+1)}$, and the symplectic eigenvalues are given by:

$$v_{\mp} = \left[\sqrt{(a+b)^2 - 4c^2} \mp (b-a)\right]/2$$
$$= \sqrt{\left(N_s + N_s^{\cdot} + 1\right)^2 - 4TN_s(N_s+1)} \mp \left(N_s^{\cdot} - N_s\right). \tag{34}$$

The corresponding expression for the entanglement assisted channel capacity is given by:

$$C_{EA} = g(N_s) + g(N_s^{\cdot}) - \left[g\left(\frac{v_+ - 1}{2}\right) + g\left(\frac{v_- - 1}{2}\right)\right]. \tag{35}$$

Let us first evaluate the capacity improvement of the proposed optical hybrid-based joint detection scheme over Holevo capacity.

For channel transmissivity $T = 0.1$, average number of background photons $N_b = 20$, and the average signal photon number $N_s = 10^{-3}$, from Fig. 9 we conclude that the proposed scheme for

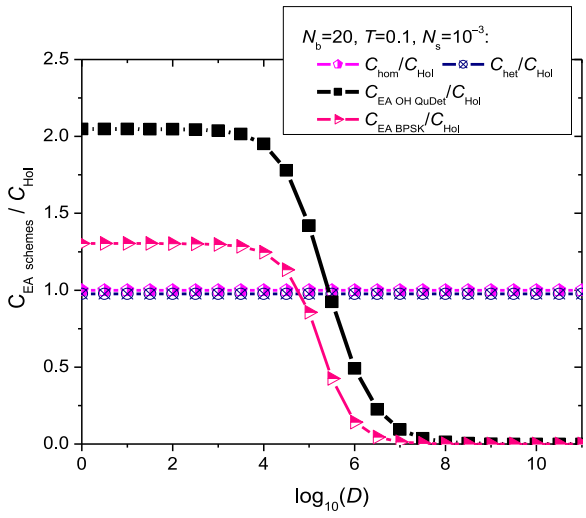

Fig. 9. The capacity improvements of proposed EA schemes over Holevo capacity vs. number of signal-idler modes. Simulation parameters are selected as follows: channel transmissivity $T = 0.1$, average number of signal photons $N_s = 10^{-3}$, and average number of background photons $N_b = 20$.

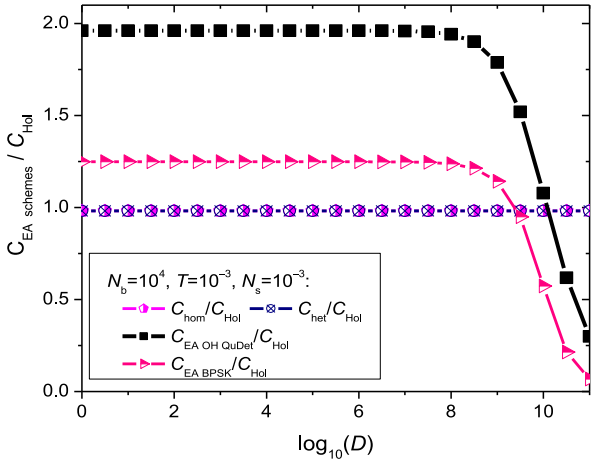

Fig. 10. The capacity improvements of proposed EA schemes over Holevo capacity vs. number of signal-idler modes. Simulation parameters are selected as follows: channel transmissivity $T = 10^{-3}$, average number of signal photons $N_s = 10^{-3}$, and average number of background photons $N_b = 10^4$.

GM outperforms the Holevo capacity by more than two times for number of signal-idler modes up to $D = 3980$. On the other hand, the BPSK based EA scheme employing receiver shown in Fig. 7 outperforms the Holevo capacity $>$1.3 times for number of signal-idler modes up to 400.

For comparison purposes, in Fig. 10 we study the capacity improvements of proposed EA schemes for the same set of parameters as Fig. 5 in ref. [8]: channel transmissivity $T = 10^{-3}$, average number of signal photons $N_s = 10^{-3}$, and average number of background photons $N_b = 10^4$. Clearly, the capacity of EA BPSK employing the joint receiver from Fig. 7 outperforms the Holevo capacity by 1.25 times for number of signal-idler modes up to 400. For number of signal-idler modes ranging from 10^8 to 10^{11} this scheme performs comparable to the OPC receiver from ref. [8], even though it has lower complexity and lower cost. On the other hand, the capacity for GM scheme employing the joint receiver from Fig. 7 outperforms the Holevo capacity by 1.96 times for number of signal-idler modes up to 5000. Interestingly enough, the capacity of proposed

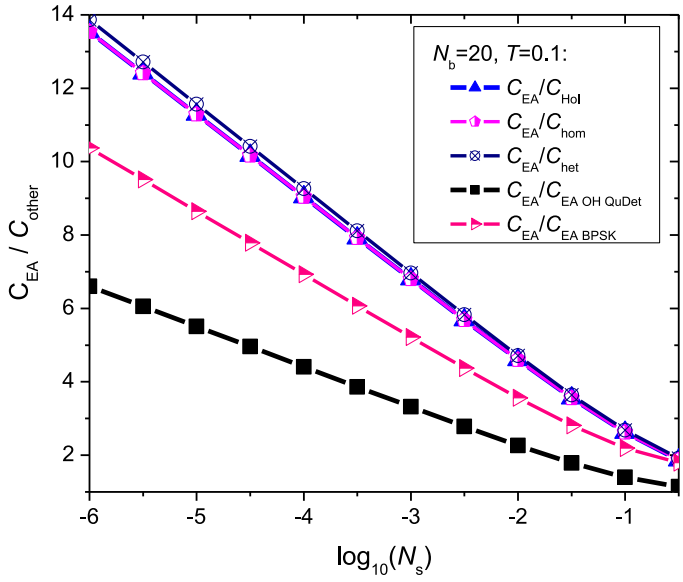

Fig. 11. The EA capacity improvements over Holevo, homodyne, heterodyne, and proposed EA optical hybrid-based joint receiver capacities vs. the average number of signal photons. Simulation parameters are selected as follows: channel transmissivity $T = 0.1$ and average number of background photons $N_b = 20$.

scheme is higher than capacity obtained for the FF-SFG receiver, see Fig. 8 in ref. [8], which has significantly higher complexity and cost. By close inspection of Figs 9 and 10, contrary to ref. [8], we conclude that for the proposed joint receiver the large number of signal-idler modes is not required; moreover, the single signal-idler pair is sufficient.

This motivates to study how the capacity of proposed scheme with GM compares against the EA capacity given by Eq. (35) and corresponding results are summarized in Fig. 11 by setting the simulation parameters as follows: channel transmissivity $T = 0.1$ and average number of background photons $N_b = 20$. The capacity of the proposed scheme with GM is significantly better compared to EA BPSK, homodyne, and heterodyne capacities.

Before concluding this section, it would be interesting to see the capacity improvements of the proposed EA schemes against the channel attenuation when the distribution channel is either perfect of imperfect, and the corresponding results are summarized in Figs. 12–13, assuming that the number of signal-idler modes is $D = 10$. Simulation parameters are provided in the text of corresponding Figures. Clearly, as shown in Fig. 12(left), for the ideal distribution channel, the EA capacity improvements over Holevo capacity are not attenuation dependent, as expected.

On the other hand, when the comparison is performed in terms of absolute chancel capacity values (expressed in bits/s/Hz), as shown in Fig. 12(right), we see that the channel capacity for the proposed quantum detectors outperforms EA BPSK (based on OPC receiver), Holevo, homodyne, and heterodyne capacities for all channel attenuations. However, it does not outperform the theoretical EA capacity, as expected, indicating that there is the space for further improvements.

When the entanglement distribution channel is imperfect, represented as the lossy and noisy Bosonic channel with transmittance $T_d = 0.5$ and average number of background photons of $N_d = 7$, from Fig. 13(left), we conclude that the improvement due to EA, over Holevo capacity, is channel attenuation dependent. When there is no attenuation in the main channel, EA BPSK (based on OPC receiver performs worse than all other capacities). The EA communication should be used when the channel attenuation is at least 10 dB. Form Fig. 13(right), we conclude the gap between the EA capacity for the proposed quantum detector and theoretical EA curve is smaller when the distribution channel is imperfect.

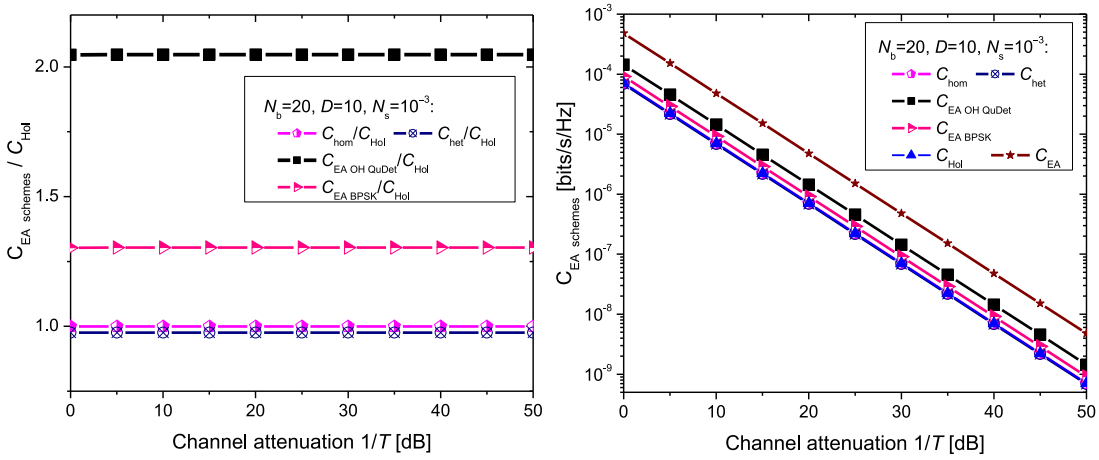

Fig. 12. The capacity improvements of proposed EA schemes over Holevo capacity vs. channel attenuation 1/T[dB] assuming that the distribution channel is ideal. Simulation parameters are selected as follows: number of signal-idler modes $D = 10$, average number of signal photons $N_s = 10^{-3}$, and average number of background photons $N_b = 20$.

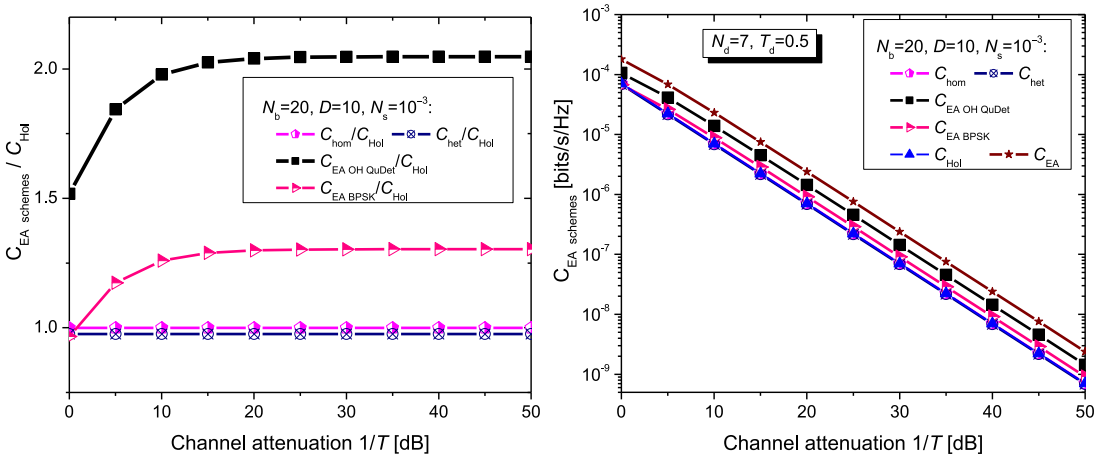

Fig. 13. The capacity improvements of proposed EA schemes over Holevo capacity vs. channel attenuation 1/T[dB] assuming that the distribution channel is imperfect with average number of background photons $N_d = 7$ and distribution channel attenuation $T_d = 0.5$. Simulation parameters are selected as follows: number of signal-idler modes $D = 10$, average number of signal photons $N_s = 10^{-3}$, and average number of background photons $N_b = 20$.

6. Concluding Remarks

Entanglement represents a unique feature for the QIP enabling new types of sensors with measurement sensitivities beating the classical limit, allowing quantum computers to solve the problems being numerically intractable for classical computers, and providing certifiable security for data transmission. In particular, the preshared entanglement between two communicating parties can be used to surpass classical communication limits and Holevo capacity in highly noisy, low-brightness regime. The EA capacity has been known for decades, nevertheless there are two key obstacles for practical applications. Firstly, the distribution of entanglement over long distances has been an outstanding challenge due to photon losses. Secondly, the optimum quantum receiver, achieving EA channel capacity, has not been fully derived yet.

In this paper, as the contribution to the second problem, several low-complexity, high-performance joint quantum receivers have been proposed, employing optical hybrids and balanced detectors, which are well known in classical coherent detection. By employing the Gaussian modulation on transmitter side and the proposed joint quantum receivers on receiver side we have demonstrated by simulations that the proposed joint detection schemes can outperform the OPA, optical phase-conjugation, and sum-frequency generation receivers. Simulation results indicate that the capacity of the proposed EA schemes, based on a single signal-idler pair, outperforms both the Holevo capacity and classical (homodyne and heterodyne) channel capacities, even when the entanglement distribution is imperfect.

References

[1] I. B. Djordjevic, *Physical-Layer Security and Quantum Key Distribution*. Cham, Switzerland: Springer Nature Switzerland AG, 2019.
[2] G. Cariolaro, *Quantum Communications*. Cham, Switzerland: Springer International Publishing, 2015.
[3] I. B. Djordjevic, *Quantum Information Processing, Quantum Computing, and Quantum Error Correction: An Engineering Approach,* 2nd ed. Elsevier/Academic, 2021.
[4] A. S. Holevo, and R. F. Werner, "Evaluating capacities of bosonic gaussian channels," *Phys. Rev. A*, vol. 63, no. 3, 2001, Art. no. 032312.
[5] A. S. Holevo, "On entanglement assisted classical capacity," *J. Math. Phys.*, vol. 43, no. 9, pp. 4326–4333, 2002.
[6] C. H. Bennett, P. W. Shor, J. A. Smolin, and A. V. Thapliyal, "Entanglement-assisted capacity of a quantum channel and the reverse shannon theorem," *IEEE Trans. Inf. Theory*, vol. 48, pp. 2637–2655, Oct. 2002.
[7] M. Sohma, and O. Hirota, "Capacity of a channel assisted by two-mode squeezed states," *Phys. Rev. A*, vol. 68, no. 2, 2003, Art. no. 022303.
[8] H. Shi, Z. Zhang, and Q. Zhuang, "Practical route to entanglement-assisted communication over noisy bosonic channels," *Phys. Rev. Appl.*, vol. 13, no. 3, 2020, Art. no. 034029.
[9] R. V. Meter, and S. J. Devitt, "The path to scalable distributed quantum computing," *IEEE Comput.*, vol. 49, Sep. 2016, Art. no. 9.
[10] Z. Zhang, and Q. Zhuang, "Distributed quantum sensing," *Quantum Sci. Technol.*, 2021. *arXiv:2010.14744*.
[11] A. M. Childs, "Secure assisted quantum computation," *Quantum Inf. Computation*, vol. 5, no. 6, pp. 456–466, 2005.
[12] Q. Zhuang, Z. Zhang, and J. H. Shapiro, "Optimum mixed-state discrimination for noisy entanglement-enhanced sensing," *Phys. Rev. Lett.*, vol. 118, no. 4, 2017, Art. no. 040801.
[13] Z.-Y. J. Ou, *Quantum Optics for Experimentalists*. Singapore; Hackensack, NJ, USA; London, UK: World Scientific Publishing Company, 2017.
[14] I. B. Djordjevic, *Advanced Optical and Wireless Communications Systems*. Cham, Switzerland: Springer International Publishing AG, 2018.
[15] R. Simon, "Peres-Horodecki separability criterion for continuous variable systems," *Phys. Rev. Lett.*, vol. 84, no. 12, 2000, Art. no. 2726.
[16] L.-M. Duan, G. Giedke, J. I. Cirac, and P. Zoller, "Inseparability criterion for continuous variable systems," *Phys. Rev. Lett.*, vol. 84, no. 12, 2000, Art. no. 2722.
[17] A. Serafini, "Multimode uncertainty relations and separability of continuous variable states," *Phys. Rev. Lett.*, vol. 96, no. 11, 2006, Art. no. 110402.
[18] S. Pirandola, A. Serafini, and S. Lloyd, "Correlation matrices of two-mode bosonic systems," *Phys. Rev. A*, vol. 79, no. 5, 2009, Art. no. 052327.
[19] C. Weedbrook, *et al.*, "Gaussian quantum information," *Rev. Mod. Phys.*, vol. 84, no. 2, pp. 621–669, 2012.